© 2018. This manuscript version is made available under the CC-BY-NC-ND 4.0 license http://creativecommons.org/licenses/by-nc-nd/4.0/
The published version is available via https://doi.org/10.1016/j.bios.2018.07.014.

Highlights

• A well-designed biointerface enabled the selective and quantitative detection of dopamine using a potentiometric biosensor.

• Dopamine-templated molecularly imprinted polymer was synthesized on the extended Au gate electrode of a field-effect transistor.

• The thickness of the dopamine-templated molecularly imprinted polymer was controlled to ca. 60 nm by surface-initiated atom transfer radical polymerization.

• A detection range of 40 nM–20 μM and a detection limit of 96 nM for dopamine detection were achieved while the smaller responses to other catecholamines.

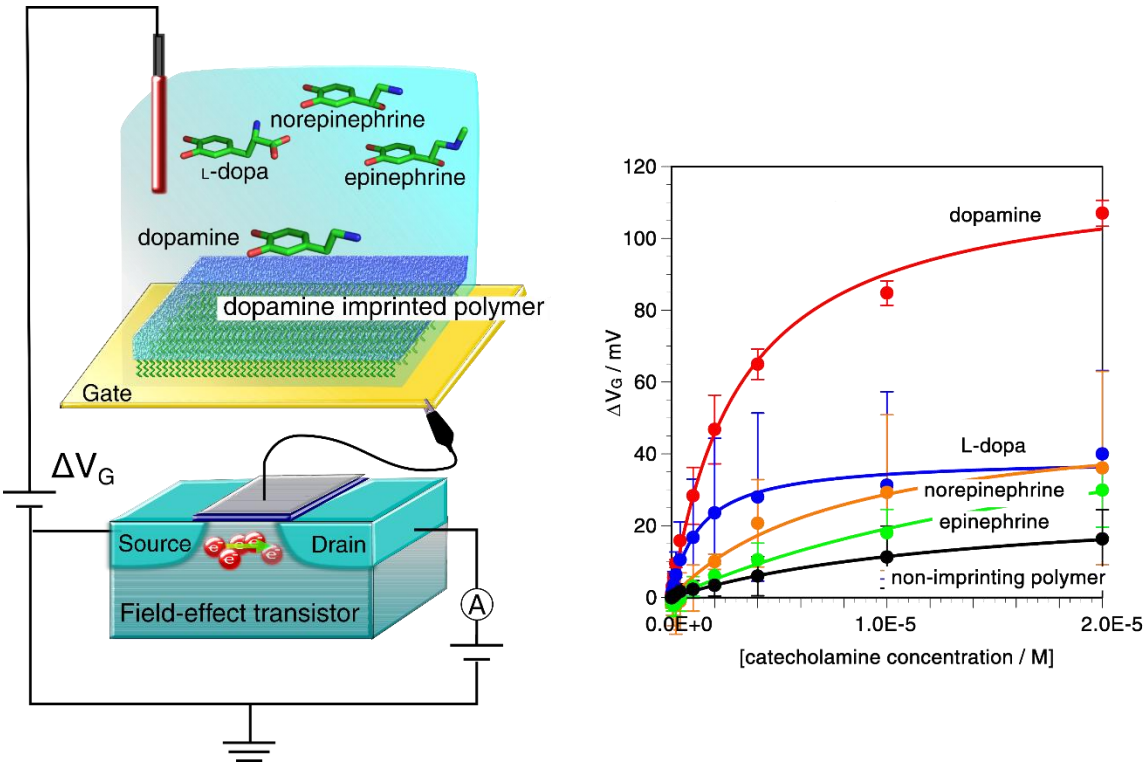

Graphic abstract

Manuscript
Click here to view linked References

Well-designed dopamine-imprinted polymer interface for selective and quantitative dopamine detection among catecholamines using a potentiometric biosensor

Taira Kajisa[a*], Wei Li[b], Tsuyoshi Michinobu[b], Toshiya Sakata[c]

a PROVIGATE Inc., The University of Tokyo Entrepreneur Plaza, 7-3-1 Hongo, Bunkyo-ku, Tokyo 113-0033, Japan

b Department of Materials Science and Engineering, Tokyo Institute of Technology, 2-12-1 Ookayama, Meguro-ku, Tokyo 152-8552, Japan

c Department of Materials Engineering, School of Engineering, The University of Tokyo, 7-3-1 Hongo, Bunkyo-ku, Tokyo 113-8656, Japan

Corresponding Authors

*Taira Kajisa

E-mail: kajisa@provigate.com

Abbreviations:

MIP, molecularly imprinted polymer; MOSFET, metal-oxide-semiconductor field-effect transistor; DA, dopamine; LD, L-dopa; NE, norepinephrine; EP, epinephrine.

ABSTRACT

We report a well-designed biointerface enabling the selective and quantitative detection of dopamine (DA) using a potentiometric biosensor. To enhance the detection selectivity of DA, a DA-templated molecularly imprinted polymer (DA–MIP) was synthesized on the extended Au gate electrode of a field-effect transistor (FET) biosensor. For a quantitative DA analysis, the thickness of the DA–MIP was controlled to ca. 60 nm by surface-initiated atom transfer radical polymerization (SI-ATRP). In this process, the DA–MIP was copolymerized with vinylphenylboronic acid (vinyl-PBA), inducing molecular charges at the biointerface of the FET gate electrode. These charges were generated by the diol-binding between PBA and dopamine (a catecholamine), and were directly detected as a change in surface potential. In fact, the surface potential at the gate of the DA–MIP-coated FET responded significantly to DA added at concentrations ranging from 40 nM to μM, whereas that of a non-imprinted polymer (NIP)-coated FET hardly changed over this range. Moreover, by measuring the kinetic parameters and electrochemical properties of well-designed devices with various added catecholamines, we confirmed that the DA–MIP-coated FET biosensor selectively and quantitatively detects DA.

Keywords:

catecholamine, dopamine, molecularly imprinted polymer, field-effect transistor, surface-initiated atom transfer radical polymerization

1. Introduction

Catecholamines are distributed in the adrenal medulla, brain, and sympathetic nerves (Bulbring and Burn, 1949; Von Euler and Hamberg, 1949; Goldenberg et al., 1949; Weinshilboum et al., 1971; Emlen et al., 1972; Brown et al., 1972). They play an important role as neurotransmitters in the central nervous system, and are secreted as adrenal medullary hormones in the blood, raising the blood pressure and blood sugar level (Guttmann et al., 1963; Moore et al., 1965; Tempel and Leibowitz, 1994). Starting from tyrosine, catecholamines are metabolized successively to L-dopa (LD), dopamine (DA), norepinephrine (NE), and epinephrine (EP) in the metabolic pathway. Among these metabolites, DA is a treatment modality in acute congestive heart failure and renal failure, so is a useful compound in the pharmacological field (Durairaj and Haywood, 1978; Lokhandwala and Barrett, 1982; Varriale and Mossavi, 1997). The addition of a carboxyl group, hydroxyl group, and methyl group to the side chain of DA yields LD, NE, and EP, respectively. Catecholamine concentrations in blood and urine have been determined by high-performance liquid chromatography (HPLC), which quantifies the catecholamine concentration *in vivo* (Mori, 1981; Helm et al., 1982; Minami et al., 1984).

Several methods that distinguish among the different catecholamine structures have been reported. As a non-enzymatic detection method, catecholamines can be specifically detected by molecularly imprinted polymer (MIP), a biomimetic material that mimics the enzyme–substrate relationship. Molecular cavities in polymer have been fabricated by polymerizing a monomer mixed with a substrate (Wulff and Sarhan, 1972; Wulff et al., 1973; Andersson et al., 1985; Sellergren et al., 1985). To improve the specificity of MIPs, researchers have attempted to increase the crosslinker density and design the monomer composition by exploiting the covalent

bonds between the functional monomer and the substrate, the ionic interaction, the electrostatic interaction, and the hydrogen bonds (Wulff, 1995). MIP-based catecholamine detection methods include an indirect method intermediated by an enzyme and chromophores, and a swelling–shrinking-based detection method (Suedee et al, 2006; Lakshmi et al., 2009; Mao et al., 2011). However, direct electrochemical detection by a MIP has been rarely reported. For quantitative DA measurement, this technique requires precise control of the polymerization conditions and the film thickness of the MIP at the electrode interface (Panasyuk-Delaney et al., 2001).

Potentiometric electrochemical devices based on field-effect transistors (FETs) can realize non-labeled, quantitative, low-cost biosensors (Bergveld, 1970; Fromherz and Offenhausser, 1991; Lahav et al., 2001). By virtue of the field effect, a charge change in the gate vicinity of an FET manifests as a change in the source–drain current up to the threshold voltage of the FET, after which the source–drain current remains constant. FET-based techniques have quantified ions, proteins, nucleic acids, and charged cells with high sensitivity (Sakata et al., 2004; Star et al., 2006; Sakata and Miyahara, 2008; Sakata and Matsuse, 2017; Sakata et al., 2013; Rothberg et al., 2011; Kajisa and Sakata, 2014). Furthermore, an extended-gate FET, in which the gate electrode is separated from the semiconductor device, allows free choice of the gate electrode material, which can be grown by a diverse range of surface modification methods (Sakata et al., 2005). Our group quantitatively detected various saccharides at concentrations of order 10 μM using a chemically modified extended-gate FET with a modified Au gate electrode. In that study, the gate was modified by a phenylboronic acid self-assembled monolayer (PBA-SAM) (Kajisa and Sakata, 2014). The FET with the PBA-SAM-coated gate directly measured the changes in the negative charge as the boron atoms altered from a tertiary to quaternary structure. This change was driven by diester binding of PBA with sugar (a diol compound). Using the same

PBA equilibrium principle, glucose was also detected at high sensitivity by an FET with a hydrogel-coated gate, formed by polymerizing hydrogel-containing vinyl-PBA on an extended Au gate electrode (Kajisa and Sakata, 2017). As a PBA molecule can also bind to the diol group of catecholamines, the PBA equilibrium mechanism has also been exploited in catecholamine detection (Hansson et al., 1978; Paugam et al., 1994).

Against this background, we propose that DA can be directly measured with high sensitivity and selectivity among structurally similar catecholamines using a DA-templated MIP–FET. To quantify the affinity and binding constant of the DA–MIP, we precisely control the thickness and adhesiveness of the MIP layer at the Au electrode surface by surface-initiated atom transfer radical polymerization (SI-ATRP), which directly forms a hydrogel nanolayer on the Au substrate.

2. Experimental section

2.1. Chemicals and materials

All chemicals were obtained from commercial suppliers and used without further purification. 3-(3,4-Dihydroxyphenyl)-L-alanine (LD), 3-hydroxytyramine hydrochloride (DA), L-noradrenaline bitartrate (NE), and L-adrenaline (EP) were purchased from Tokyo Kasei Industry (Tokyo, Japan). The MIP was fabricated from different monomers: *N*-[3-(dimethylamino)propyl]methacrylamide (DMAPM, Sigma-Aldrich), 4-vinylphenylboronic acid (VPBA, Tokyo Kasei Industry), or ethylene glycol dimethacrylate (EGDM, Wako Pure Chemical). The solvent was *N*,*N*-dimethylformamide (DMF, Wako Pure Chemical). The initiator for atom transfer radical polymerization (ATRP) was bis[2-(2-bromoisobutyryloxy)undecyl] disulfide (Sigma-Aldrich). The catalysts were $CuBr_2$ and tris(2-pyridylmethyl)amine (TPMA), and the reducing agent was ascorbic acid (Nacalai Tesque). Phosphate-buffered saline without bivalent ions (PBS-, Thermo Fisher Scientific) was used as the buffer solution. An n-channel metal-oxide-semiconductor field-effect transistor (MOSFET, 2N7002) was purchased from NXP Semiconductors. Ultrapure water (Ul-pure, Komatsu Electronics Co., Ltd.) was used in all experiments.

2.2. Controlled polymerization of DA-MIP on Au surface by surface-initiated ATRP (SI-ATRP)

A nanolayer of DA-MIP was fabricated by SI-ATRP, a controlled living radical polymerization method. First, an ATRP initiator (Br-SAM) was formed by immersing an Au electrode in 1 mM bis[2-(2-bromoisobutyryloxy)undecyl] disulfide/ethanol solution. The DA–MIP was polymerized by mixing 105 mM of DMAPM, 120 mM of VPBA, 540 mM of EGDM, and 188 mM of DA. The monomers were dissolved in DMF/water (7.5 ml/2.5 ml), and DA was

added following degassing by N_2 bubbling to prevent the self-oxidation of DA. A non-imprinted polymer (NIP) was prepared as described for DA–MIP but omitting the DA. After mixing the monomers and DA for 1 h with N_2 bubbling, $CuBr_2$ and TPMA were added to the final concentrations of 1 and 5 mM in the monomer solution, respectively. Finally, 10 mM of ascorbic acid (reducing agent) was added to the solution in a glove box, before immersing the Br-SAM-coated Au electrode. Polymerization was performed at 40 °C for 18 h. After polymerization, the treated Au substrate was washed in methanol and water to remove the unreacted monomers and DA, then immersed in 0.1 M HCl and 50 %(v/v) methanol for more than 3 days to remove the DA from the pre-MIP hydrogel. At the end of this period, the DA template was formed in the MIP hydrogel.

2.3. Elemental analyses by X-ray photoelectron spectroscopy

The surface elemental compositions of Au, Au with an immobilized ATRP initiator, and DA–MIP-modified Au were analyzed by X-ray photoelectron spectroscopy (XPS) (JPS-9010MC, JEOL). Excitation X-rays were produced from a monochromatic Al Kα X-ray source at a take-off angle of 90°.

2.4. Estimation of polymer thickness on Au surface by ellipsometric analysis

The thicknesses of the Br-SAM, polymerized DA–MIP, and NIP on the Au electrode were calculated by ellipsometric measurements using a rotating ellipsometer (model M2000U, J.A. Woollam Co., Inc.) and WVASE32 software. The wavelength of the incident light ranged from 200 to 1600 nm, and the incidence angle was 65, 70, 75, or 80°. To calculate the thickness of each layer, the experimentally obtained spectrum was fitted by the Cauchy model, which

approximates the dispersion of the refractive index. The thickness was determined as the average of at least three measurements obtained from different substrates or locations.

2.5. Electrochemical characterization of the Au gate electrode with a DA–MIP membrane

To clarify the characteristics of the Au gate electrode with a polymerized DA–MIP membrane, we measured the capacitance changes in the fabricated polymer layer at each step of the ATRP process, and compared the impedance changes in DA–MIP and NIP as the DA concentration was varied. The capacitances were measured by an LCR meter (E4980A, Keysight technologies) operated at 50 Hz and a bias voltage of 10 mV. The measurement buffer was PBS buffer (pH 7.4) and the reference electrode was an Ag/AgCl electrode. The impedance was measured by an electrochemical analyzer (614E, BAS Instruments) over a wide range of frequencies (10 mHz to 1 MHz). The measurement buffer was PBS buffer (pH 7.4) containing 1 mM of potassium ferricyanide/potassium ferrocyanide as redox mediators. The reference and counter electrodes were an Ag/AgCl electrode and a platinum electrode, respectively. To determine the pK_a of the PBA molecules in DA–MIP, a DA–MIP-coated Au electrode was connected to an n-channel MOSFET device (input capacitance: 31 pF) and the shift in the threshold voltage (ΔV_T) at a drain current (I_D) of 4 mA and a drain voltage (V_D) of 2 V was measured using a semiconductor parameter analyzer (B1500A, Keysight Technologies). During the ΔV_T measurements, the 100 mM sodium phosphate buffer was increased from pH 5 to 12, with or without 10 μM DA, and the pK_a was calculated by fitting the ΔV_T versus pH data with a sigmoidal curve.

2.6. Evaluation of affinity to catecholamines in FET with DA-MIP-coated gate

The DA-substrate specificity of the FET with a DA–MIP-coated gate was evaluated in a mixture of catecholamines using a real-time monitoring system. For this purpose, 500 μl of PBS buffer (pH=7.4) was poured onto a DA–MIP-coated gate surface equipped with a 12-mm-diameter glass ring, and equilibrated until the gate surface potential was stabilized. After stabilizing the gate surface potential, each catecholamine was gradually titrated to a final concentration range of 10 nM to 20 μM. To suppress the spike signals in the gate surface potential induced by sample addition, the introduced volume was 1/100 of the total volume of the measurement solution. The change in surface potential (ΔV_{out}) at the gate was measured at a constant I_D of 100 μA using a source follower circuit (with the Ag/AgCl reference electrode grounded). The detected ΔV_{out} was thus regarded as the change in the source–gate voltage (ΔV_S), which equals the $-\Delta V_T$ of an FET. This system monitors the surface potential of the FET in real time.

3. Results and discussion

3.1. SI-ATRP of DA-MIP on the extended Au gate electrode

To fabricate the FET with the DA–MIP-coated gate, a MIP hydrogel was synthesized on the surface of the Au electrode, following the modification of bromo-terminated alkanethiol SAMs as the ATRP initiator. **Schemes 1a and 1b** illustrate the FET with the DA–MIP-coated gate and the chemical structure of the DA–MIP obtained by SI-ATRP, respectively. To prepare a thin layer of DA–MIP, the DA template molecule was mixed into a solution containing a functional monomer (vinylphenylboronic acid). Similarly to other catecholamines, DA rapidly self-polymerizes while forming the ring structure of 5,6-dihydroxyindole by an oxidation process (Liebscher et al., 2013; Shi et al., 2016). To prevent such self-oxidation of DA, the DA–MIP was polymerized in a nitrogen atmosphere with all air strictly removed. The surface of each Au electrode modified with the SI-ATRP initiator–SAM and DA–MIP was analyzed by XPS, ellipsometry, and capacitance measurements. The elemental composition of the Au surface changed during each step of the chemical modification (XPS analysis; see **Fig. S1** in the Supplementary information). The peak intensities of elemental carbon and bromine increased after coating the SI-ATRP initiator on the Au electrode, while the Au peak decreased. Furthermore, MIP synthesis by SI-ATRP increased the intensity of the carbon peak and simultaneously decreased the intensities of the bromo group and Au peaks. These results confirm that SI-ATRP formed a polymer layer on the Au gate electrode of the FET. To more deeply understand the DA–MIP layer, the layer thickness was determined by fitting to an optical model using an ellipsometer. The experimental spectra of the azimuth (Ψ), defining the difference between the p- and s-polarized light angles, were well fitted to the spectra simulated by the Cauchy model (**Fig. S2** in the Supplementary information). From these data, the thicknesses of

the ATRP-initiator SAMs, NIP, and DA–MIP were determined as 1.6 ± 0.0 nm, 57.3 ± 1.3 nm, and 61.3 ± 4.1 nm, respectively. Furthermore, the capacitance of each organic layer on the Au surface decreased from 1.60 μF (electric double-layer on the bare Au surface) to 1.24 μF in the ATRP-initiator–SAM-modified Au electrode, 450 nF in the NIP-coated Au electrode, and 190 nF in the DA–MIP-coated Au electrode. The capacitance of the interface of the organic-layer-coated Au electrode (C_{int}) is thought to decrease with increasing thickness of the modified organic layer, and is generally described as

$$C_{\text{int}} = \varepsilon_{OL} \frac{S}{d_{OL}}, \quad (1)$$

where ε_{OL} and d_{OL} denote the relative permittivity and thickness of the modified organic layer, respectively. The thickness and capacitance of each layer are tabulated in **Table S1**. The theoretical relative permittivities calculated from the thicknesses and capacitances were approximately 3 in the Br–SAM layer, 58 in the NIP/Br–SAM layer, and 20 in the DA–MIP/Br–SAM layer on the Au electrode. The relative permittivity of the densely packed Br–SAM was similar to those of other alkanethiol SAMs, and those of the hydrogels in the DA–MIP and NIP layers were raised by water absorption and consequent swelling (Rampi et al., 1998; Esch et al., 1999; Yeow et al., 2010). The relative permittivity was lower in DA–MIP than in NIP despite the nearly identical thicknesses of the two layers. This may be explained by differences in the polymer compositions and structures of the random block copolymer. After complexing with DA, a large proportion of the VPBA monomer in DA–MIP was negatively charged, whereas in the NIP monomer solution, most of the VPBA was neutral (Yu and Eisenberg, 1997). Consequently, in the MIP case, VPBA was copolymerized with DMAPM via electrostatic interaction with the amino-group side chain of DMAPM, whereas the NIP synthesis was largely affected by π–π

interactions between the VPBA molecules. Therefore, the different dielectric constants of DA–MIP and NIP might be explained by the morphological differences in the hydrogels of a molecularly imprinted polymer and a non-imprinted random copolymer.

3.2. Electrochemical characterization of Au electrode with DA-MIP membrane

The DA–MIP-coated Au electrode was electrochemically characterized by electrochemical impedance spectroscopy (EIS), and the semiconductor properties of the FET with a DA–MIP-coated gate were examined using a semiconductor parameter analyzer. First, the layered interfaces of the NIP- and DA–MIP-coated Au electrodes were clarified by EIS. The impedance of each Au surface was measured by changing the DA concentration. According to the modulus of impedance in the NIP- and DA–MIP-coated Au electrodes, which increases with increasing frequency at lower frequencies (below Hz order), the redox reaction of the mediator proceeded at the Au electrode (**Fig. S3** in the Supplementary information). **Fig. 1** shows Nyquist plots of the NIP- and DA–MIP-coated Au electrodes, which resolve the impedance into real and imaginary parts, in the frequency range from 10 mHz to 1 MHz. A typical capacitive semicircle with a time constant ($\tau = RC$) appears at higher frequencies in both plots, owing to electron transfer induced by the redox reaction of the ferricyanide/ferrocyanide mediator with the Au electrode. For the DA–MIP-coated Au electrode in the absence and presence of 100 nM DA, the diagonal line at lower frequencies corresponds to the diffusion-limited Warburg impedance (**Fig. 1b**). Therefore, the equivalent circuit may be a series connection of the charge transfer resistance and the Warburg impedance, in parallel with the electric double-layer capacitance of the Au electrode (**Fig. 1b, inset**). Increasing the DA concentration enlarged the capacitive semicircle for the DA–MIP-coated Au electrode, but not for the NIP-coated Au electrode. Assuming the resistance–

capacitance (RC) circuit model, the charge transfer resistance (R_{CT}) was estimated from the intersection of the semicircle plot with the X-axis, and the electric double-layer capacitance (C_{EDL}) was calculated from the frequency corresponding to the vertex of the semicircle (f_{max}) and R_{CT} as

$$f_{max} = \frac{1}{2\pi R_{CT} C_{EDL}} . \quad (2)$$

Table 1 summarizes the parameters of the RC circuits of the NIP- and DA–MIP-coated Au electrodes at different DA concentrations. As the DA concentration increased, the C_{EDL} remained unchanged in both electrodes, whereas R_{CT} increased in the DA–MIP-coated Au electrode but not in the NIP-coated Au electrode. This indicates gradual inhibition of the redox reaction by the binding of DA and PBA molecules in the MIP, which blocks the DA–MIP cavities and prevents the redox mediator from passing through the DA–MIP membrane. On the other hand, the R_{CT} values were several times larger in the NIP-coated Au electrode than in the DA–MIP-coated Au electrode, and were unchanged by DA addition. This behavior might occur because the redox mediator cannot easily reach the Au surface through the NIP membrane (**Fig. 1a**). The EIS analysis clarified and electrochemically characterized the polymer thin film on the Au electrode of the NIP- and DA–MIP-coated Au electrodes, and the DA binding behavior in DA–MIP was observed as an impedance change.

The DA–MIP-coated gate FET was further characterized using a semiconductor parameter analyzer. **Fig. 2** plots the ΔV_T values as functions of pH with and without DA addition. The V_T versus pH curve was successfully fitted by a sigmoidal function (Eq. (3)), which is based on the Hill equation (Hill, 1910):

$$\Delta V_T = \Delta V_{T\max} - \frac{\Delta V_{T\max} + \Delta V_{Tbase}}{1+(\frac{pH}{pK_a})^n}, \quad (3)$$

where $\Delta V_{T\,base}$ and $\Delta V_{T\,max}$ are the approximate minimum and maximum ΔV_T, respectively, n is the Hill coefficient, and pK_a is the acid dissociation constant of DA–MIP. The pK_a values of DA–MIP in the absence and presence of 10 μM DA were calculated as 10.2 and 8.14, respectively. The difference might be attributable to equilibrium between the PBA and the diol compound. PBA has four different equilibrium states in association with the diol compound, and the boron atom is negatively charged in PBA itself and upon binding to the diol compound (**Scheme 1c**). In the PBA of DA–MIP, the changing negative charge of the boron atoms induced a ΔV_T shift in the positive direction. Thus, the above values denote the pK_a of PBA itself and the pK_a of the PBA–DA complex. The pK_a of PBA in DA–MIP (state 2 in **Scheme 1c**) was higher than the pK_a of PBA molecules (8.8) reported in earlier studies (Springsteen and Wang, 2002; Yan et al., 2004). It is suspected that the pK_a of a PBA molecule tethered in DA–MIP on the Au surface differs from that of PBA molecules in bulk solution. The hydrolysis reaction field should be more limited for immobilized PBA molecules in the local environment of the MIP hydrogel at the Au interface than for PBA molecules, which can freely move through bulk solution. However, in the PBA–DA complex, DA addition shifted the sigmoidal curve to near-neutral pK_a (**Fig. 2**) and increased the variation range of V_G around neutral pH (state 3 in **Scheme 1c**). This suggests that the DA–MIP FET detects DA as the gate potential changes at the pH of biological fluids.

3.3. DA-specific detection in catecholamines using FET with DA–MIP-coated gate

A thin layer of DA–MIP was successfully polymerized onto an Au electrode by SI-ATRP and characterized by electrochemical methods. The DA–MIP-coated Au electrode was then

employed as the gate electrode of an extended-gate FET, and its specificity and sensitivity to DA were examined. **Fig. 3a** plots the ΔV_{out} values of the FET with the DA–MIP-coated gate at different concentrations of added catecholamines, and of the FET with the NIP-coated gate in the presence of DA. In the DA–MIP coated-gate FET, the ΔV_{out} decreased in a stepwise manner as the DA concentration increased from 40 nM to 20 μM. Owing to the field effect, the negatively charged PBA–DA complexes formed by incorporating DA in the DA–MIP membrane affected the electron density at the source–drain channel in the MOSFET. Consequently, the gate surface potential decreased at constant I_{SD}. This result was supported by the semiconductor parameter analysis of the NIP- and DA–MIP-coated gate FETs in the presence of different DA concentrations (**Fig. S4** in the Supplementary information). As shown in the I_D–V_G curves, the V_T increased with increasing DA concentration in the DA–MIP-coated gate FET, but hardly changed in the NIP-coated gate FET. This result indicates that the gate surface potential of the DA–MIP FET responded to DA addition, and detected DA concentrations as low as 40 nM. Conversely, the ΔV_{out} values of the DA–MIP-coated gate FET were markedly lower after LD, NE, and EP addition than after DA addition. ΔV_{out} was also lower in the NIP-coated gate FET after DA addition. Considering the EIS analysis and FET measurements of the DA–MIP and NIP FETs, we infer that the ATRP-based DA–MIP successfully imprinted the shape of DA at the interface of the Au electrode, enabling the electrochemical detection of the charge changes as DA binds to PBA.

The operation of an FET in the unsaturated region is generally described by

$$I_D = \mu C_{OX} \frac{W}{L} \left[(V_G - V_T) V_D - \frac{1}{2} V_D^2 \right] , \qquad (4)$$

where I_D is the drain current, μ is the electron mobility in the channel, C_{OX} is the gate oxide capacitance, and $\frac{W}{L}$ is the channel width-to-length ratio. V_D and V_G are the applied drain–source

and gate–source voltages, respectively, and V_T is the threshold voltage, given by (Sakata and Matsuse, 2017)

$$V_T = E_{ref} - \psi_0 + \chi^{sol} - \frac{\phi_{si}}{q} - \frac{Q_{it}+Q_f+Q_B}{C_{OX}} + 2\phi_f \ . \quad (5)$$

In Eq. (5), E_{ref} is the reference electrode potential relative to the vacuum potential, $(-\psi_0 + \chi^{sol})$ describes the potential at the interface of the electrolyte and the Au gate electrode (here, χ^{sol} is the surface dipole moment of the solution, which can be assumed constant), $\frac{\phi_{si}}{q}$ is the silicon electron work function, Q_{it}, Q_f, and Q_B are the charges per unit area of the interface traps, the fixed oxides and the bulk depletion layer, respectively, and ϕ_f is the Fermi potential difference between the doped bulk silicon and intrinsic silicon.

Accounting for the capacitance and charge of the DA–MIP membrane on the Au gate electrode, Eq. (3) is modified as follows:

$$V_T = E_{ref} - \psi_0 + \chi^{sol} - \frac{\phi_{si}}{q} - \frac{Q_{it}+Q_f+Q_B+Q_{MIP}}{C_{Com}} + 2\phi_f \ , \quad (6)$$

with

$$C_{Com} = \frac{C_{OX} \cdot C_{MIP}}{C_{OX}+C_{MIP}} = \frac{C_{OX}}{1+\frac{C_{OX}}{C_{MIP}}} \ . \quad (7)$$

where Q_{MIP} is the charge in the DA–MIP membrane and C_{Com} is the combined capacitance of the gate oxide (C_{OX}) and the DA–MIP membrane (C_{MIP}) on the Au electrode. In this study, C_{MIP} hardly changed after DA addition because the MIP hydrogel was hydrophilic, meaning that C_{Com} was almost unchanged after DA adsorption. Moreover, the change in the interfacial potential ($\Delta\psi_0$) at the electrolyte/Au gate-electrode interface was constant because the ionic concentration (i.e., the pH) was steadied by the buffer solution. The quantities E_{ref}, $\frac{\phi_{si}}{q}$, Q_{it}, Q_f, Q_B, and ϕ_f should also be unchanged by molecular recognition events at the MIP interface. Thus, the signal

response obtained by the FET sensor almost entirely reflects the change in V_T (ΔV_T), so we should evaluate ΔQ_{MIP} using Eq. (6) with the above considerations.

The reversible interaction between DA and PBA in the MIP membrane is

$$\mathrm{DA} + \mathrm{PBA} \leftrightarrow \mathrm{DA \cdot PBA^-}. \quad (8)$$

The rate of formation of the $\mathrm{DA \cdot PBA^-}$ complex at time t is written as

$$\frac{d[DA \cdot PBA^-]}{dt} = k_a[DA][PBA] - k_d[DA \cdot PBA^-], \quad (9)$$

where k_a and k_d are the association and dissociation rate constants, respectively. At time t, $[PBA] = [PBA]_0 - [DA \cdot PBA^-]$, where $[PBA]_0$ is the concentration of PBA at $t = 0$. Substituting this expression into Eq. (9) gives

$$\frac{d[DA \cdot PBA^-]}{dt} = k_a[DA]([PBA]_0 - [DA \cdot PBA^-]) - k_d[DA \cdot PBA^-]. \quad (10)$$

In this study, the charge Q_{MIP} was derived from Reaction (8), so is proportional to the formation of the $\mathrm{DA \cdot PBA^-}$ complex in the DA–MIP membrane. Meanwhile, Q_{max} is proportional to the PBA concentration in the DA–MIP membrane, which indicates the capacity of the immobilized ligand. Therefore, Eq. (10) is modified to

$$\frac{dQ_{MIP}}{dt} = k_a[c](Q_{max} - Q) - k_d Q = k_a[c]Q_{max} - (k_a[c] + k_d), \quad (11)$$

where $\frac{dQ_{MIP}}{dt}$ is the rate of formation of the associated complex ($\mathrm{DA \cdot PBA^-}$) in the DA–MIP membrane (on the gate) and $[c]$ is the concentration of the analyte (DA) in the solutions. Integrating Eq. (11), we obtain

$$Q_{MIP}^t = \frac{k_a[c]Q_{max}[1-e^{-\left((k_a[c]+k_d)t\right)}]}{k_a[c]+k_d} = \frac{[c]Q_{max}}{[c]+1/K_a}\left[1 - e^{-\left((K_a[c]+1)t\right)}\right], \quad (12)$$

where K_a is the binding constant of DA and PBA (k_a/k_d) in the DA–MIP membrane. From Eq. (12), we have $Q_{MIP}^{t=0} = 0$. Considering Eq. (6), the ΔV_T after a certain reaction time t is given by

$$\Delta V_T(=-\Delta V_{out}) = -\frac{\Delta Q_{MIP}^t}{C_{Com}} = -\frac{[c]\Delta V_{out}^{max}}{[c]+\frac{1}{K_a}}\left[1-e^{-((K_a[c]+1)t)}\right] \approx -\frac{[c]\Delta V_{out}^{max}}{[c]+1/K_a}, \quad (13)$$

where $\Delta V_{out}^{\max}$ is the maximum change in surface potential induced by $\Delta Q_{\max}$, which is proportional to the number of binding sites. In this study, ΔV_{out} at the gate was measured at constant I_{D} assuming the source follower circuit in **Fig. 3a**. Therefore, the detected ΔV_{out} was regarded as the change in V_{GS}, which equals $-\Delta V_{\text{T}}$ at constant I_{D}.

Based on the above considerations, the electrical signal in the whole FET circuit should obey the Langmuir adsorption model. As ΔV_{out}^{L} was determined by ΔV_{out} at 300 seconds after each DA addition, t in the Langmuir term can be set to a large value. Therefore, the substrate specificity of DA–MIP to each catecholamine was quantitatively evaluated by the equation of adsorption equilibrium. **Fig. 3b** shows the ΔV_{out}^{L} versus concentration plots for each catecholamine from the data shown in **Fig. 3a**. The parameters of the Langmuir fitting curve are given in **Table 2**. The dependence of output voltage on DA concentration clearly differs between DA–MIP and NIP with DA addition. The saturated amount of DA adsorption (recorded as ΔV_{max}^{L}) and K_{a} were 4.3 and 4.4 times higher, respectively, in the DA–MIP-coated gate FET than in the NIP-coated gate FET. In the DA–MIP-coated gate FET, the ΔV_{max}^{L} was clearly higher after DA addition than after LD addition, although the binding constant of LD was twice that of DA. In LD, the carboxyl group in the vicinity of a catechol provides many disester–PBA binding sites, so the ΔV_{max}^{L} appears to be higher for LD than for NE and EP (Friedman et al., 1974; Takahashi et al., 2008). Secor and Glass (2004) determined the K_{a} of PBA in the presence of different catecholamines using a fluorescence chemosensor. In their study, the K_{a} was 1.5 and 2 times higher for NE and EP than for DA, respectively, suggesting that the affinity of PBA to DA was lower than the other catecholamines. However, in the present study, the PBA in the DA–MIP-coated gate FET

showed higher affinity to DA than to NE and EP. From the quantitative evaluation of the DA–MIP-coated gate FET, we concluded that a DA–MIP-coated gate FET can potentially select DA from a mixture of catecholamines.

To assess the sensitivity of the DA–MIP-coated gate FET to different catecholamines, we calculated the limit of detection (LOD) for each catecholamine in terms of the Kaiser limit (Kaiser, 1947). The LOD was calculated by regression analysis of the linear region, which maximizes the square of the correlation factor (R^2) of the ΔV_{out} versus catecholamine concentration plot (**Fig. S5** in the Supplementary information). The estimated LODs of DA–MIP were 96 nM for DA, 150 nM for LD, 179 nM for NE, and 355 nM for EP. In previous HPLC and fluorescence spectroscopy analyses, the dopamine concentrations were identified as sub-nM to 100 nM in plasma, saliva, and tears, and as μM-order in urine (Cuche et al., 1985; Cuche et al., 1986). The DA–MIP-coated gate FET in the present study has sufficient DA sensitivity to monitor urine, and nearly sufficient DA sensitivity to monitor other analytes. Therefore, the DA–MIP-coated gate FET can potentially measure DA in various body fluids with high sensitivity and specificity in the future.

4. Conclusions

We investigated the fundamental properties of a DA–MIP-coated gate FET. A nano layer of DA–MIP was modified on a gate electrode by SI-ATRP while controlling its thickness. The DA–MIP-coated Au electrode was electrochemically characterized by capacitance, impedance, and FET measurements. The gate surface potential of the DA–MIP-coated gate FET clearly decreased when the added DA concentration exceeded 40 nM, and the responses to DA addition clearly differed from the responses to other catecholamines. The gate potential versus concentration relationships for each catecholamine were quantified by the Langmuir adsorption isotherm, suggesting that DA–MIP recognizes the side-chain functional group of the catecholamine and specifically captures DA. The binding phenomenon manifests as an electrical signal in the FET. The MIP–FET combination provides a potentially useful sensor for identifying analogous structures and for specifically detecting DA in body fluids.

Acknowledgment

This study was partly supported by the New Energy and Industrial Technology Development Organization (NEDO) under the Ministry of Economy Trade and Industry (METI) of Japan. Part of this work was conducted at the Advanced Characterization Nanotechnology Platform of the University of Tokyo, supported by the "Nanotechnology Platform" of the Ministry of Education, Culture, Sports, Science and Technology (MEXT), Japan. The authors wish to thank Assistant Professor K. Konishi of the University of Tokyo in Japan for his help in the ellipsometry experiment.

References

Andersson, L., Ekberg, B., Mosbach, K., 1985. Tetrahedron Lett. 26, 3623-3624.

Bergveld, P., 1970. IEEE Trans. Biomed. Eng. 17, 70-71.

Brown, J.H., Makman, M.H., 1972. Proc. Natl. Acad. Sci. U.S.A. 69, 539-543.

Bulbring, E., Burn, J.H., 1949. Nature 163, 363.

Cuche, J.-L., Prinseau, J., Selz, F., Ruget, G., Baglin, A., 1986. Kidney international 30, 566-572.

Cuche, J., Prinseau, J., Selz, F., Ruget, G., Tual, J., Reingeissen, L., Devoisin, M., Baglin, A., Guédon, J., Fritel, D., 1985. Hypertension 7, 81-89.

Durairaj, S.K., Haywood, L.J., 1978. Clin. Pharmacol. Therapeutics 24, 175-185.

Yu, Y., Eisenberg, A., 1997. J. Am. Chem. Soc. 119, 8383-8384.

Emlen, W., Segal, D.S., Mandell, A.J., 1972. Science 175, 79-82.

Esch, M., Sukhorukov, V.L., Kuerschner, M., Zimmermann, U., 1999. Biopolym. 50, 227-237.

Friedman, S., Pace, B., Pizer, R., 1974. J. Am. Chem. Soc. 96, 5381-5384.

Fromherz, P., Offenhausser, A., 1991. Science 252, 1290.

Goldenberg, M., Faber, M., Alston, E.J., Chargaff, E.C., 1949. Science 109, 534-535.

Guttmann, L., Munro, A.F., Robinson, R., Walsh, J.J., 1963. Paraplegia 1, 4-18.

Hansson, C., Agrup, G., Rorsman, H., Rosengren, A.-M., Rosengren, E., 1978. J. Chromatogr. A 161, 352-355.

Helm, G., Owman, C., Rosengren, E., Sjoberg, N.O., 1982. Biol. Reprod. 26, 553-558.

Hill, A.V., 1910. J. Physiol. 40, 4-7.

Kaiser, H., 1947. Spectrochim. Acta 3, 40-67.

Kajisa, T., Sakata, T., 2014. ChemElectroChem 1, 1647-1655.

Kajisa, T., Sakata, T., 2017. Sci. Technol. Adv. Mater. 18, 26-33.

Lahav, M., Kharitonov, A.B., Willner, I., 2001. Chem. Eur. J. 7, 3992-3997.

Lakshmi, D., Bossi, A., Whitcombe, M.J., Chianella, I., Fowler, S.A., Subrahmanyam, S., Piletska, E.V., Piletsky, S.A., 2009. Anal. Chem. 81, 3576-3584.

Liebscher, J., Mrowczynski, R., Scheidt, H.A., Filip, C., Hadade, N.D., Turcu, R., Bende, A., Beck, S., 2013. Langmuir 29, 10539-10548.

Lokhandwala, M.F., Barrett, R.J., 1982. J. Auton. Pharmacol. 2, 189-215.

Mao, Y., Bao, Y., Gan, S., Li, F., Niu, L., 2011. Biosens. Bioelectron. 28, 291-297.

Minami, M., Sano, M., Togashi, H., Endo, T., Saito, I., Nomura, A., Saito, H., Nakamura, N., Kurimoto, F., Sakurai, H., et al., 1984. Nihon Yakurigaku Zasshi 83, 17-31.

Moore, K.E., McCarthy, L.E., Borison, H.L., 1965. J. Pharmacol. Exp. Ther. 148, 169-175.

Mori, K., 1981. J. Chromatogr. 218, 631-637.

Panasyuk-Delaney, T., Mirsky, V.M., Ulbricht, M., Wolfbeis, O.S., 2001. Anal. Chim. Acta 435, 157-162.

Paugam, M.-F., Valencia, L.S., Boggess, B., Smith, B.D., 1994. J. Am. Chem. Soc. 116, 11203-11204.

Rampi, M.A., Schueller, O.J., Whitesides, G.M., 1998. Appl. Phys. Lett. 72, 1781-1783.

Rothberg, J.M., Hinz, W., Rearick, T.M., Schultz, J., Mileski, W., Davey, M., Leamon, J.H., Johnson, K., Milgrew, M.J., Edwards, M., Hoon, J., Simons, J.F., Marran, D., Myers, J.W., Davidson, J.F., Branting, A., Nobile, J.R., Puc, B.P., Light, D., Clark, T.A., Huber, M., Branciforte, J.T., Stoner, I.B., Cawley, S.E., Lyons, M., Fu, Y., Homer, N., Sedova, M., Miao, X., Reed, B., Sabina, J., Feierstein, E., Schorn, M., Alanjary, M., Dimalanta, E., Dressman, D., Kasinskas, R., Sokolsky, T., Fidanza, J.A., Namsaraev, E., McKernan, K.J., Williams, A., Roth, G.T., Bustillo, J., 2011. Nature 475, 348-352.

Sakata, T., Miyahara, Y., 2008. Anal. Chem. 80, 1493-1496.

Sakata, T., Matsuse, Y., 2017. Genes Cells 22, 203-209.

Sakata, T., Kamahori, M., Miyahara, Y., 2005. Jpn. J. Appl. Phys. 44, 2854-2859.

Sakata, T., Matsumoto, S., Nakajima, Y., Miyahara, Y., 2005. Jpn. J. Appl. Phys. 44, 2860-2863.

Sakata, T., Saito, A., Mizuno, J., Sugimoto, H., Noguchi, K., Kikuchi, E., Inui, H., 2013. Anal. Chem. 85, 6633-6638.

Secor, K.E., Glass, T.E., 2004. Org. Lett. 6, 3727-3730.

Sellergren, B., Ekberg, B., Mosbach, K., 1985. J. Chromatogr. A 347, 1-10.

Shi, L., Santhanakrishnan, S., Cheah, Y.S., Li, M., Chai, C.L., Neoh, K.G., 2016. ACS Appl. Mater. Interfaces 8, 33131-33138.

Springsteen, G., Wang, B.H., 2002. Tetrahedron 58, 5291-5300.

Star, A., Tu, E., Niemann, J., Gabriel, J.C.P., Joiner, C.S., Valcke, C., 2006. Proc. Natl. Acad. Sci. U.S.A. 103, 921-926.

Suedee, R., Seechamnanturakit, V., Canyuk, B., Ovatlarnporn, C., Martin, G.P., 2006. J. Chromatogr. A 1114, 239-249.

Takahashi, S., Kurosawa, S., Anzai, J.-i., 2008. Electroanalysis 20, 816-818.

Tempel, D.L., Leibowitz, S.F., 1994. J. Neuroendocrinol. 6, 479-501.

Varriale, P., Mossavi, A., 1997. Clinical cardiology 20, 627-630.

Von Euler, U.S., Hamberg, U., 1949. Nature 163, 642.

Weinshilboum, R.M., Thoa, N.B., Johnson, D.G., Kopin, I.J., Axelrod, J., 1971. Science 174, 1349-1351.

Wulff, G., 1995. Angew. Chem. Int. Ed. 34, 1812-1832.

Wulff, G., Sarhan, A., 1972. Angew. Chem. 84, 364-364.

Wulff, G., Sarhan, A., Zabrocki, K., 1973. Tetrahedron Lett. 14, 4329-4332.

Yan, J., Springsteen, G., Deeter, S., Wang, B., 2004. Tetrahedron 60, 11205-11209.

Yeow, Y.K., Abbas, Z., Khalid, K., Rahman, M.Z., 2010. Amer. J. Appl. Sci. 7, 270-276.

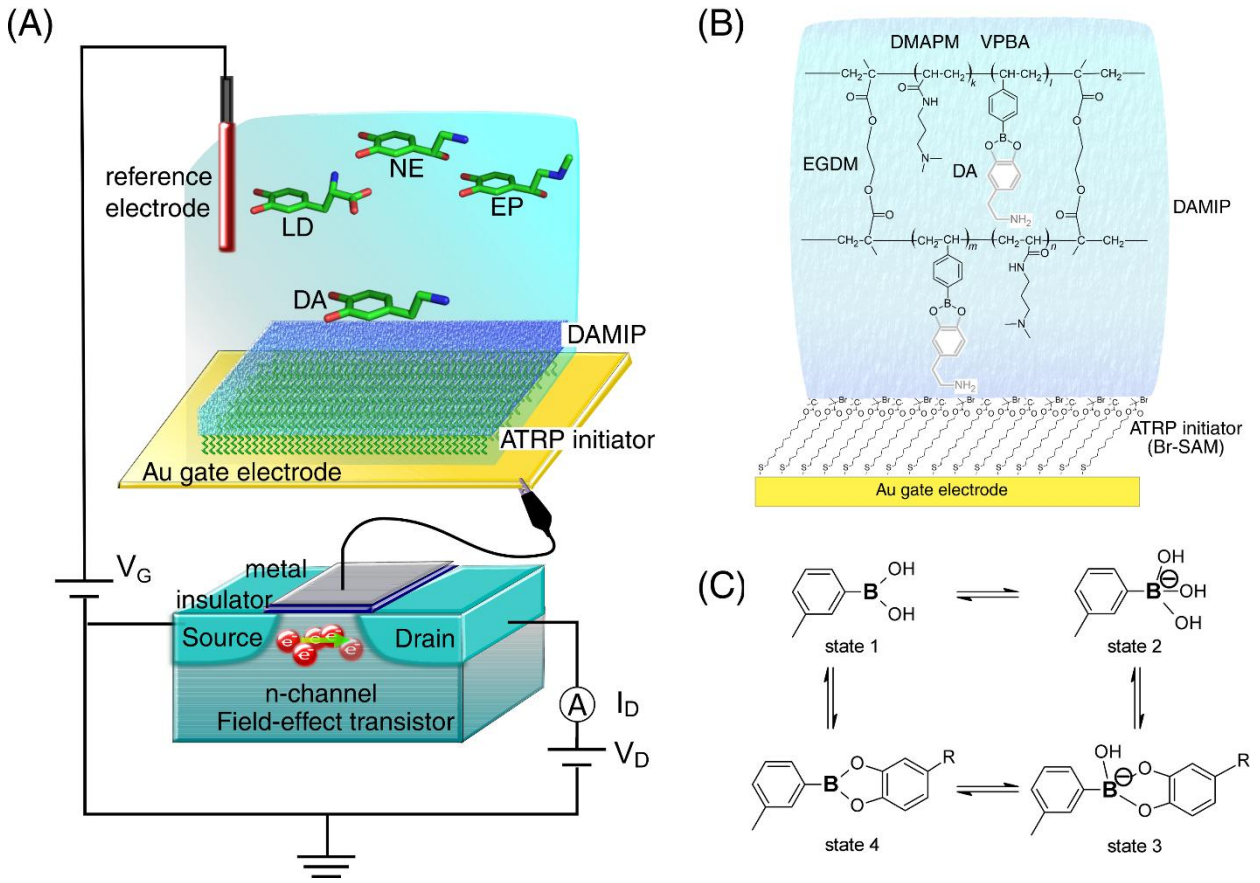

Scheme 1. Conceptual structure of DA–MIP-coated gate FET. (A) Schematic diagram of DA–MIP-coated gate FET. The DA–MIP-coated Au gate electrode was extended from MOSFET. (B) Chemical composition of DA–MIP coated by SI-ATRP on an Au electrode. Bromo-terminated alkanethiol SAM was tethered as ATRP initiator on the Au electrode, and then DA–MIP was synthesized with forming VPBA-DA complexes. (C) Equilibrium between phenylboronic acid derivative and diol compound.

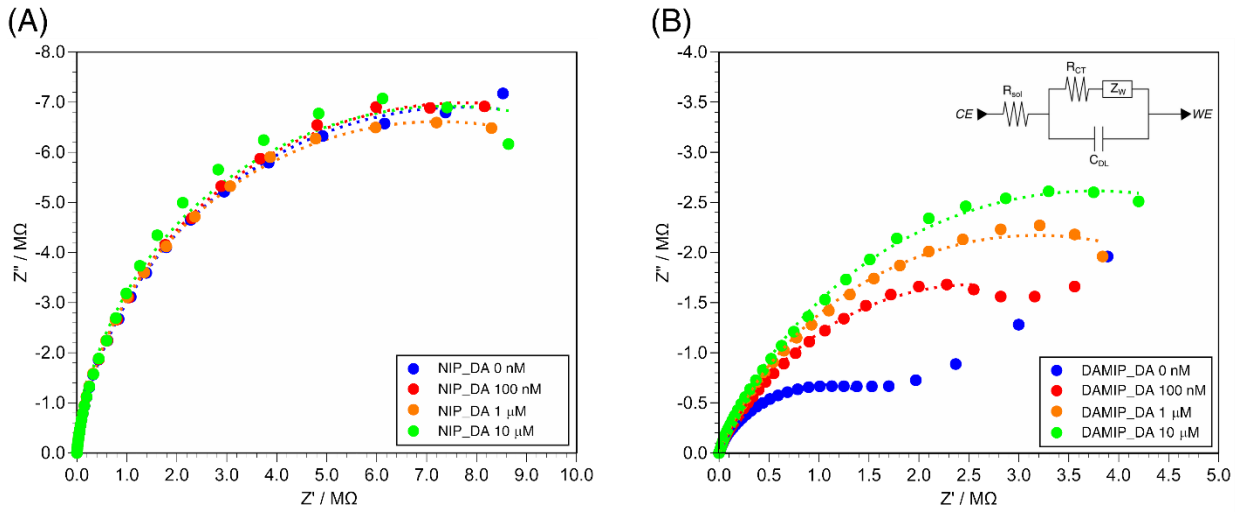

Figure 1. Impedance analyses for NIP- and DA–MIP-coated Au electrodes. Nyquist plots of (A) NIP- and (B) DA–MIP-coated Au electrodes at different concentrations of DA from 0 nM to 10 μM. The inset in (B) shows the equivalent circuit of DA–MIP-coated Au surface (CE: counter electrode, R_{sol}: resistance of solution, R_{CT}: resistance of charge transfer, Z_w: Warburg impedance, C_{DL}: capacitance of electric double layer, WE: working electrode).

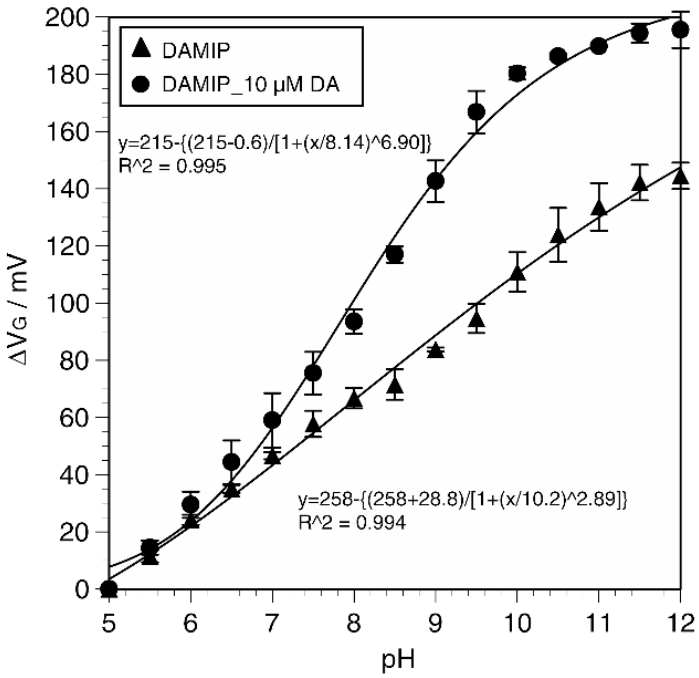

Figure 2. Threshold gate voltage shift (ΔV_G) for DA–MIP-coated gate FET at 4 mA of I_D obtained from I_D-V_G curve with changes in pH from 5 to 12. Sigmoidal plots of DA–MIP-coated gate FET were obtained without DA in each pH solution (triangle), and with 10 μM of DA (circle). Each approximated formula of sigmoidal plots was shown in the figure.

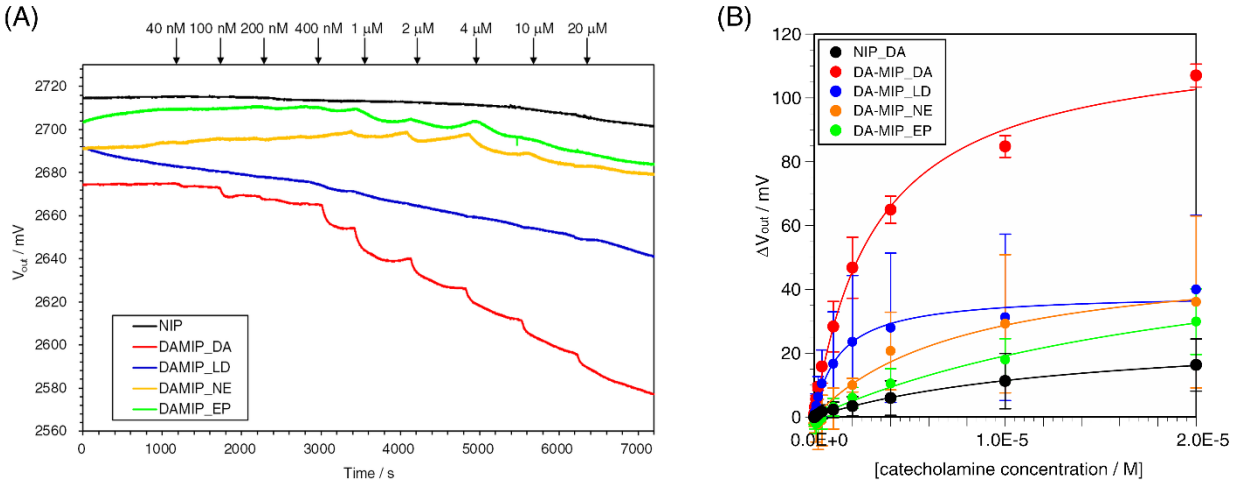

Figure 3. (A) Change in gate surface potential (V_{out}) of DA–MIP-coated gate FET with different concentrations of catecholamines at a constant I_D (100 μA). Four types of catecholamines, DA (red line), LD (blue line), NE (orange line) and EP (green line), were added at each time indicated by arrows. The NIP-coated gate FET was used as a control upon adding DA (black line). (B) Plots of shift in gate surface potential (ΔV_{out}) at different concentrations of added catecholamines based on the data shown in **Fig. 3A**. Approximate curves were fitted by Langmuir adsorption isotherm. ΔV_{out} were analyzed for the DA–MIP-coated gate FETs, where four types of catecholamines, DA (red), LD (blue), NE (orange) and EP (green), were added with different concentrations. The NIP-coated gate FET was used as a control upon adding DA (black).

Table 1. Impedimetric parameters in RC circuit of NIP- and DA–MIP-coated Au electrodes at different concentrations of DA.

	Dopamine concentration (μM)	parameters		
		f_{max} (mHz)	C_{EDL} (μF)	R_{CT} (MΩ)
NIP	0	14.7	0.70	15.5
	0.1	14.7	0.70	15.5
	1	14.7	0.75	14.5
	10	14.7	0.73	14.9
DA–MIP	0	56.2	1.37	2.07
	0.1	21.5	1.43	5.17
	1	14.7	1.70	6.36
	10	14.7	1.44	7.52

Table 2. Kinetic parameters calculated from the approximate curves shown in **Fig. 3b**, which were based on Langmuir model.

Polymer-additive catecholamine	Kinetic parameters		
	ΔV_{max}^{L} (mV)	K_a (10^5 M^{-1})	R^2
NIP_DA	27.5	0.71	0.996
DA–MIP_DA	119	3.11	0.995
DA–MIP_LD	63.6	7.75	0.986
DA–MIP_NE	51.5	1.26	0.974
DA–MIP_EP	38.8	4.33	0.981

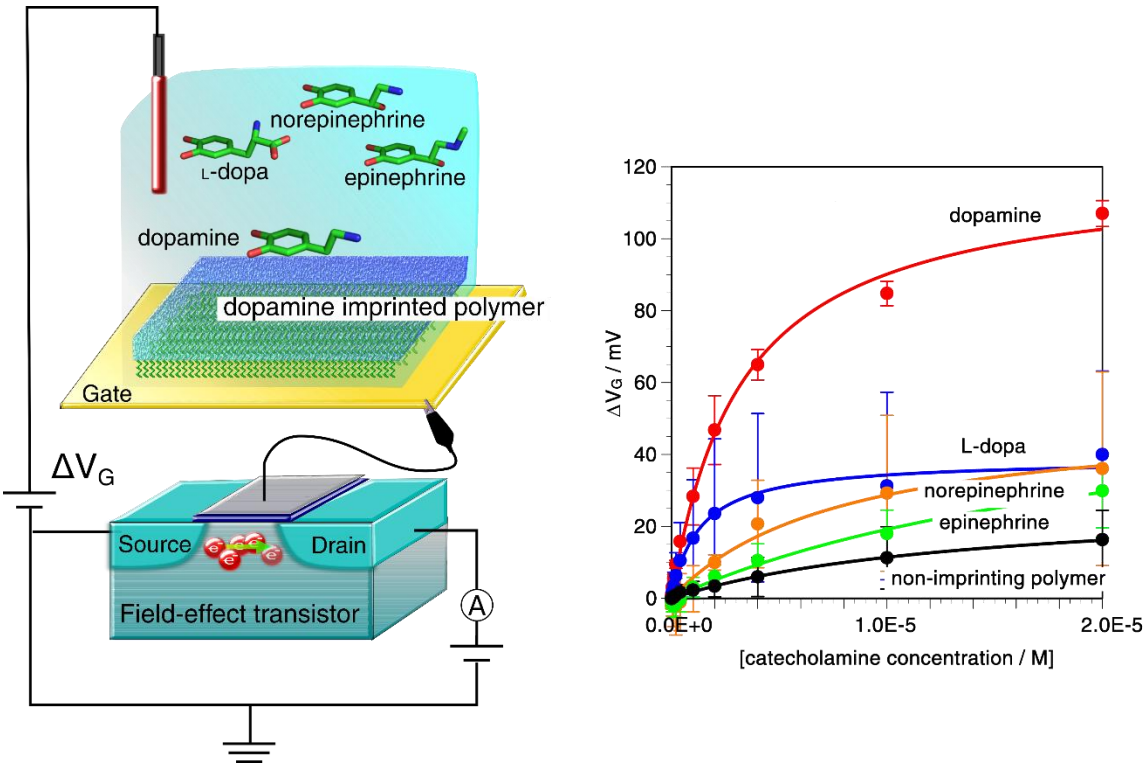

Graphic abstract

Figure(s)

Click here to download high resolution image

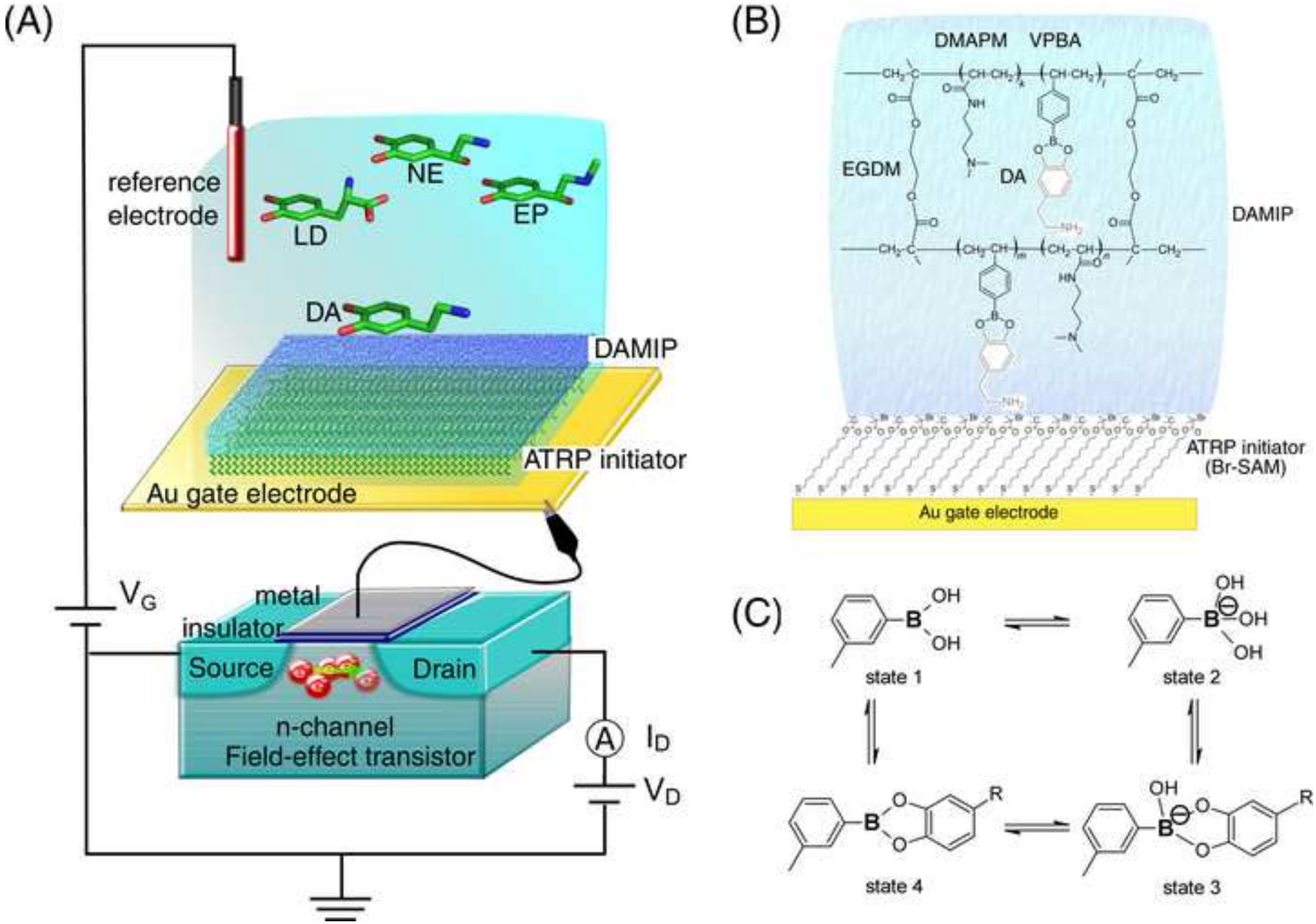

Figure(s)

Click here to download high resolution image

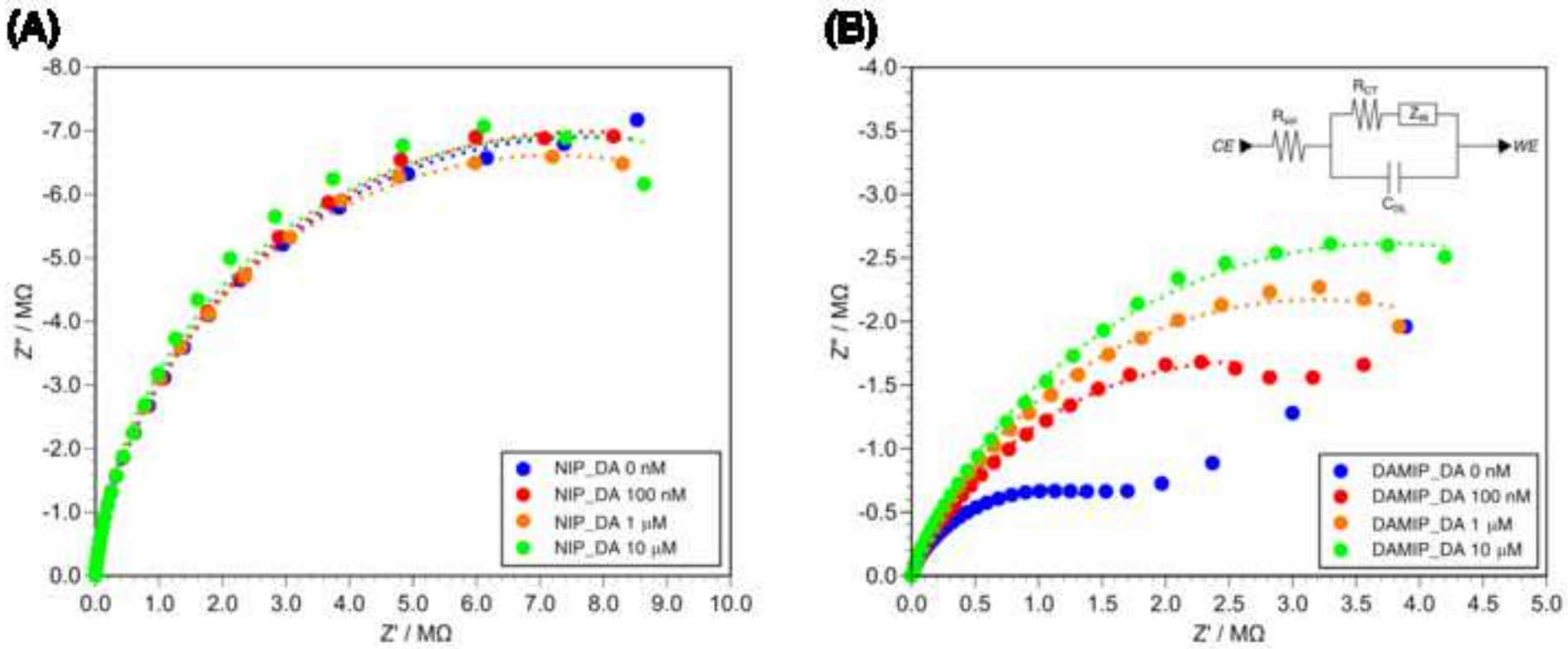

Figure(s)

Click here to download high resolution image

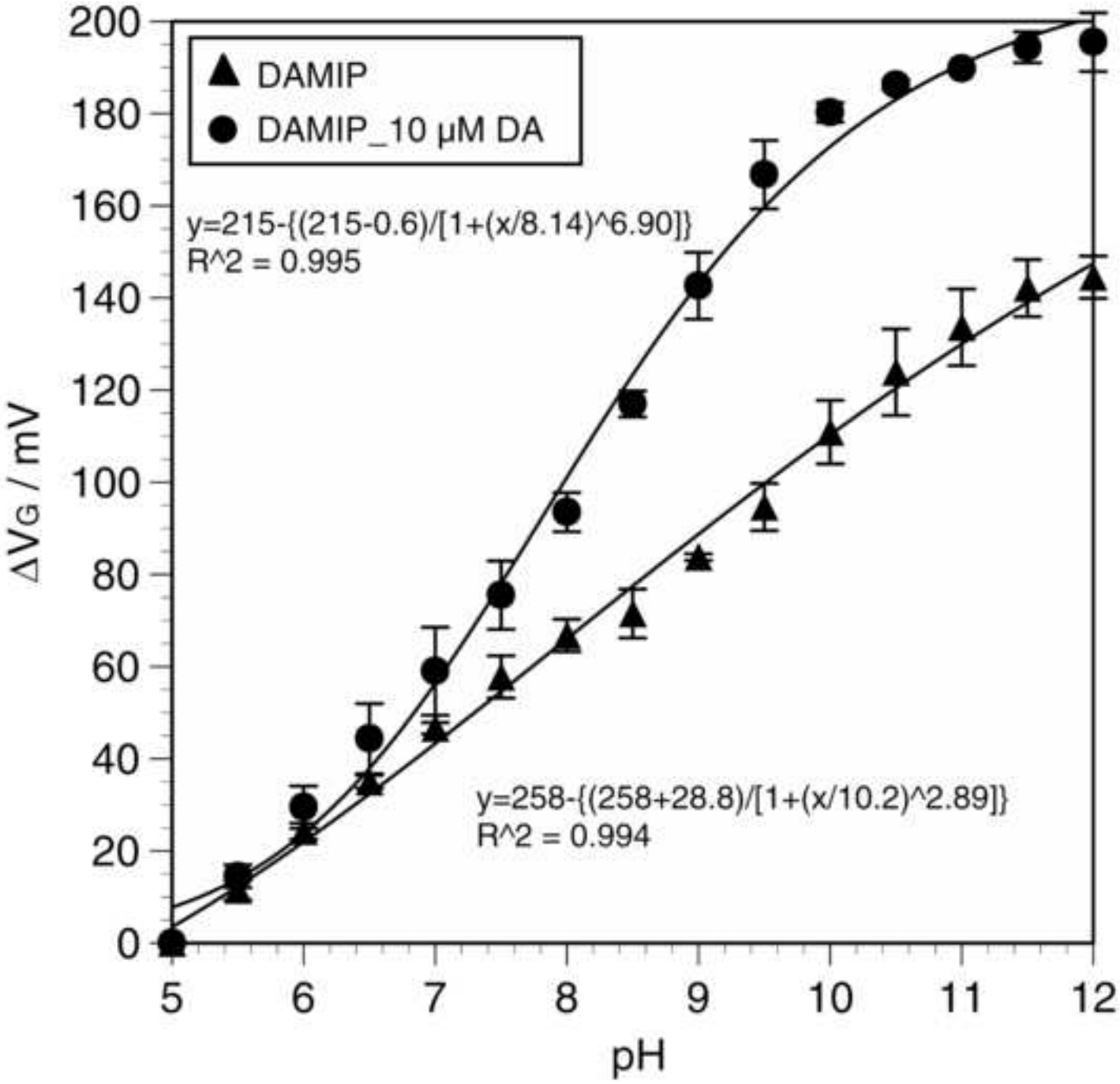

Figure(s)

Click here to download high resolution image

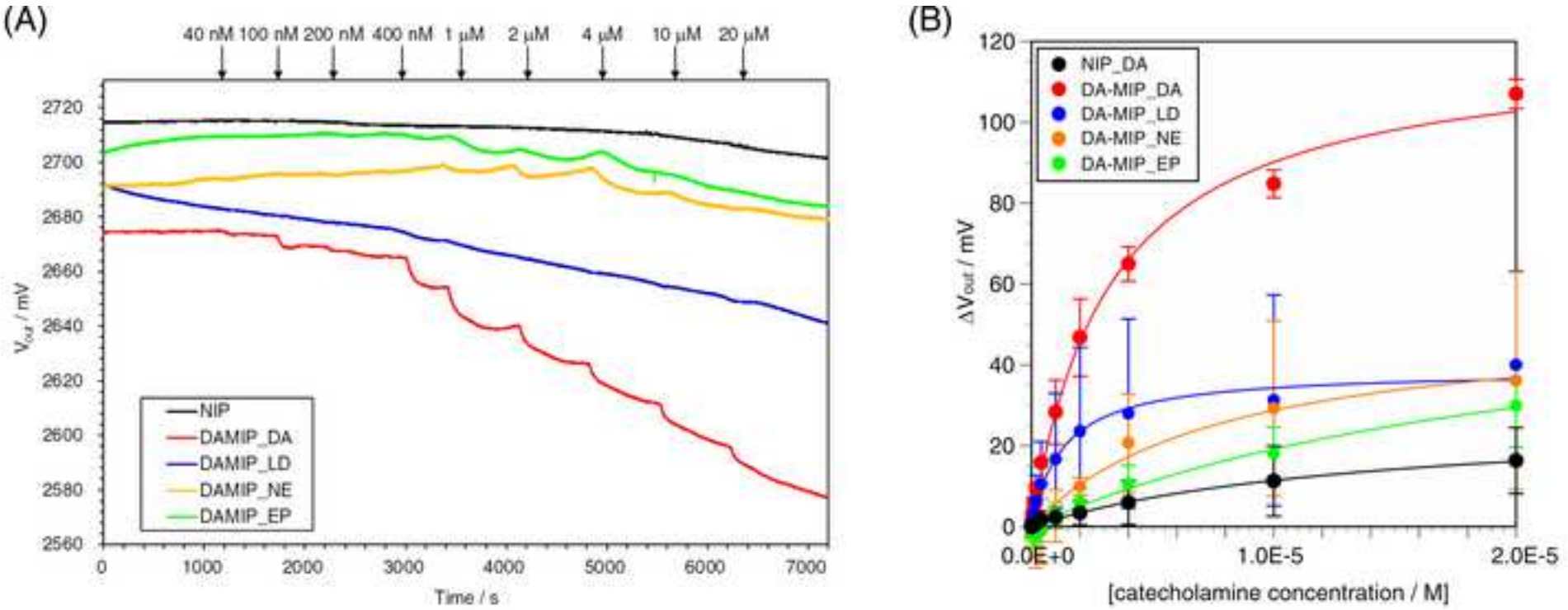

Table 1. Impedimetric parameters in RC circuit of NIP- and DA–MIP-coated Au electrodes at different concentrations of DA.

	Dopamine concentration (μM)	parameters		
		f_{max} (mHz)	C_{EDL} (μF)	R_{CT} (MΩ)
NIP	0	14.7	0.70	15.5
	0.1	14.7	0.70	15.5
	1	14.7	0.75	14.5
	10	14.7	0.73	14.9
DA–MIP	0	56.2	1.37	2.07
	0.1	21.5	1.43	5.17
	1	14.7	1.70	6.36
	10	14.7	1.44	7.52

Table 2. Kinetic parameters calculated from the approximate curves shown in **Fig. 3b**, which were based on Langmuir model.

Polymer-additive catecholamine	Kinetic parameters		
	ΔV_{max}^{L} (mV)	K_a (10^5 M^{-1})	R^2
NIP_DA	27.5	0.71	0.996
DA–MIP_DA	119	3.11	0.995
DA–MIP_LD	63.6	7.75	0.986
DA–MIP_NE	51.5	1.26	0.974
DA–MIP_EP	38.8	4.33	0.981

Supplementary Material

Click here to download Supplementary Material: 180220_SupplementaryMaterial.pdf